Applied Catalysis B: Environmental 194 (2016) 7–15

Contents lists available at ScienceDirect

Applied Catalysis B: Environmental

journal homepage: www.elsevier.com/locate/apcatb

Surface controlled generation of reactive radicals from persulfate by carbocatalysis on nanodiamonds

Xiaoguang Duan[a], Chao Su[a], Li Zhou[a], Hongqi Sun[a,b,*], Alexandra Suvorova[c], Taiwo Odedairo[d], Zhonghua Zhu[d], Zongping Shao[a], Shaobin Wang[a,*]

[a] Department of Chemical Engineering, Curtin University, GPO Box U1987, WA 6845, Australia
[b] School of Engineering, Edith Cowan University, 270 Joondalup Drive, Joondalup, Perth, WA 6027, Australia
[c] Centre for Microscopy, Characterization and Analysis, The University of Western Australia, Crawley, WA 6009, Australia
[d] School of Chemical Engineering, The University of Queensland, St Lucia, QLD 4072, Australia

ARTICLE INFO

Article history:
Received 21 January 2016
Received in revised form 28 March 2016
Accepted 21 April 2016
Available online 22 April 2016

Keywords:
Heterogeneous catalysis
Oxidation
Annealed nanodiamond
Hydroxyl radicals
Persulfate

ABSTRACT

Production of radicals by metal-free catalysis is expected to offer a promising oxidative reaction for remediation of emerging contaminants. In this study, novel metal-free activation of persulfate (PS) on annealed nanodiamonds (ANDs) was investigated, which demonstrated superior performances in decomposition of various pollutants to conventional metal-based catalysis. Comprehensive investigations on the effects of reaction parameters, such as solution pH, reaction temperature, initial phenol concentration, catalyst loading, PS usage, the presence of chlorine ions and humic acid, on phenol degradation were carried out. In addition, nanodiamond (ND) material optimization and reusability were also studied. Electron paramagnetic resonance (EPR) and selective organic degradation unraveled that the PS/AND system may produce both hydroxyl radicals (•OH) and sulfate radicals ($SO_4^{\bullet-}$), initialized from oxidizing water molecules on the nanodiamond surface. The carbocatalysts served as an excellent electron tunnel to facilitate the charge transfer from water or hydroxide ions to PS, and the oxidized intermediates may play a crucial role in PS activation. Electrochemical analyses in PS oxidant solution and oxygen reduction reaction (ORR) were carried out to understand O—O bond activation by the metal-free catalysis. This study provides an environmentally benign and highly efficient oxidative reaction system with reactive radicals along with insights into the metal-free PS activation process.

1. Introduction

Ongoing environmental deterioration has motivated worldwide research in green and efficient remediation to pursue the sustainable development of human society [1,2]. Green technologies integrating advanced oxidation processes (AOPs) have been developed to decompose organic contaminants using various superoxides to evolve reactive oxygen species especially for hydroxyl radicals (•OH). For instance, Fenton reactions have been widely applied in wastewater treatment, in which hydrogen peroxide (H_2O_2) is decomposed by ferrous ions (Fe^{2+}) to produce hydroxyl radicals (•OH) for AOPs. However, conventional Fenton reactions encounter some issues, for example, the instability of chemicals, pH restriction (pH ~ 3), metal leaching and flocculation [3]. In pursuit of an alternative to Fenton reaction with less inputs of chemicals and energy, extensive trials have been attempted to employ peroxymonosulfate (PMS) or persulfate (PS) salts to generate sulfate radicals, which possess a higher oxidative potential ($SO_4^{\bullet-}$, 2.5–3.1 V *vs.* •OH, 2.7 V) and better selectivity for oxidation [4]. As PS is stable and much cheaper than PMS and H_2O_2, more attention has been attracted for developing an outstanding PS-based oxidation process [5]. A variety of physical and chemical approaches have been explored to activate PS to generate sulfate radicals [6–9]. Ferrous ions, zero-valent iron (ZVI) [10,11], copper oxide (CuO), and biochar with persistent free radicals (PFRs) [5,12] have been reported for PS activation. Nanocarbons were first discovered by our group to activate PMS and PS to produce reactive species for degradation of organic contaminants (phenolics, dyes, and antibiotics) [13–15]. Wang et al. recently utilized nitrogen-doped graphene as a superb adsorbent and metal-free carbocatalyst for catalytic PS activation and removing bisphenol [16]. The work uncovered that it is the surface-bound sulfate radicals rather than the free sulfate radicals that played the crucial roles in the catalytic

* Corresponding authors.
E-mail addresses: h.sun@ecu.edu.au (H. Sun), shaobin.wang@curtin.edu.au (S. Wang).

http://dx.doi.org/10.1016/j.apcatb.2016.04.043
0926-3373/

oxidation process, and that the adsorption of pollutants and generation of sulfate radicals synergistically promotes the effectiveness of pollutant removal. In metal-catalyzed AOPs, the transition metal sites can effectively bond with PS (or PMS) molecules with empty orbitals of the outer shell and enable the electron transfer process to generate free radicals due to the variable valency nature. However, the carbocatalysis, with an electron-abundant culture, versatile functional groups and defective sites, may work differently from the metal-based system for activating superoxides. The PS/carbocatalyst have demonstrated a better controllable manner than metal-based catalysis [17]. However, this emerging catalysis is still lack of insight into the activation mechanism. The poor stability of the nanocarbons in AOPs also impedes the future applications [18].

On the other hand, industrial and domestic wastewaters usually contain high levels of salinity and diverse natural organic matters. The diversity of the contaminants requires a controllable and selective remediation. For instance, sulfate radicals ($SO_4^{\bullet -}$) would first react with Cl^- in natural wastewater to form $Cl^\bullet$ at a high reaction rate (Eq. (1), $k_{for} = 3.0 \times 10^8\ M^{-1}\ s^{-1}$), and then the $Cl^\bullet$ rapidly combines with another chloride ion to produce a chlorine radical ($Cl_2^{\bullet -}$, Eq. (2)) [19,20]. The chlorine radicals with a redox potential of 2.1 V are more selective to attack the electron-rich compounds *via* one-electron extraction, thus the efficiency would be reduced in treating electron-poor contaminants such as cyclohexanol and alkanes [21,22]. The stubborn issue of sulfate radicals with background Cl^- ions is insignificant for hydroxyl radicals at neutral and basic pHs and $Cl_2^{\bullet -}$ generation becomes remarkable only at low pHs (Eqs. (4) and (5)) [21,22]. Therefore, solutions to the above problems of both hydroxyl and sulfate radicals for practical wastewater treatment as a challenging mission have to be found out.

$$SO_4^{\bullet -} + Cl^- \leftrightarrow SO_4^{2-} + Cl^\bullet \quad (1)$$

$$Cl^\bullet + Cl^- \leftrightarrow Cl_2^{\bullet -} \quad (2)$$

$$OH^\bullet + Cl^- \leftrightarrow ClOH^{\bullet -} \quad (3)$$

$$ClOH^{\bullet -} + H^+ \leftrightarrow Cl^\bullet + H_2O \quad (4)$$

$$ClOH^{\bullet -} + Cl^- \leftrightarrow Cl_2^{\bullet -} + OH^- \quad (5)$$

Recently, nanodiamond (ND) with excellent catalytic performances and biocompatibility has become a candidate for metal-free catalysis [23–25]. In its heterogeneous catalysis, electrochemical reduction of nitrogen [26], photocatalytic water splitting [27], direct oxidation of benzene to phenol [28], and direct [29–32] or oxidative dehydrogenation (ODH) [33,34] of hydrocarbons have been reported. Further studies also indicated that modification of the sp^2 curved concentric shells of NDs with nitrogen or phosphorus could significantly enhance the catalytic activity and selectivity for ODH and selective oxidation [23,35]. Herein, for the first time, we applied annealed nanodiamonds as superb carbocatalysts to activate persulfate, and conducted mechanistic studies targeting feasible wastewater remediation. The kinetic studies at varying reaction temperature, catalyst loading, PS dosage and initial phenol concentration were carried out. The mechanisms of PS activation and radical revolution were investigated, and the possible degradation pathway was revealed by identification of the reaction intermediates. Moreover, the effects of pH, natural organic matters, and radical scavengers on oxidation efficiencies were systematically investigated. This study dedicates to providing a green, novel, and highly-efficient PS activation technology to tackle the issues in Fenton reaction and sulfate radical-based oxidation.

2. Experimental

2.1. Materials preparation and characterization

All chemicals were obtained from Sigma–Aldrich. For carbon modification, pristine nanodiamonds (NDs, particle size < 10 nm, Sigma–Aldrich, Australia) were transferred to a quartz tube and annealed at 600–1000 °C under nitrogen atmosphere for one hour to get annealed samples, denoted as AND-X (X = 600, 700, 800, 900, and 1000). Some metal oxides, Fe_3O_4, Co_3O_4, and CuO, were also prepared [17]. Ga_2O_3 and Fe_2O_3 were prepared *via* a hydrothermal method with $GaCl_3$ or $FeCl_3$ in basic conditions (pH = 10, adjusted by ammonium solution) at 180 °C for 20 h. The morphology and crystal structure of the nanodiamonds were revealed by a JEOL 2100 TEM instrument. FTIR spectra was obtained from a Bruker spectrometer. Thermo-gravimetric analysis (TGA) was recorded on a Perkin Elmer thermal analyzer in the air atmosphere with a heating rate of 5 °C/min from 50 to 900 °C. The pore structures of the carbocatalysts were estimated by the Barrett-Joyner-Halenda (BJH) method and the specific surface areas (SSAs) were calculated using the Brunauer-Emmett-Teller (BET) equation from N_2 adsorption isotherms on a TriStar II instrument. The surface chemistry of the as-made catalysts was analyzed by X-ray photoelectron spectroscopy (XPS) on a Kratos AXIS Ultra DLD machine with a monochromated Al Kα X-ray gun. Shirley background was utilized for peak fitting with C 1s calibrated to 284.5 eV for all the spectra.

2.2. Experimental procedure

Activation of persulfate by nanodiamonds and metal oxides was carried out for oxidizing various aqueous pollutants. A typical reaction was conducted in a 250 mL batch reactor with fixed amounts of phenol solution, persulfate and nanodiamonds ([catalyst] = 0.2 g/L, [PS] = 6.5 mM, [T] = 25 °C, [Phenol] = 20 mg/L, and $[pH]_{initial} = 5.9 \pm 0.1$ without a buffer solution) unless specified elsewhere. A water bath with a temperature controller was used to maintain the constant reaction temperature. Reaction solutions were withdrawn and injected into an HPLC vial through a 0.45 μm filter and mixed with ethanol ($V_{Solution}/V_{EtOH} = 2:1$) at vigorously shaking to scavenge the excessive radicals. Then, the solutions were analyzed using an UltiMate 3000 UHPLC system with an OA column (150 × 4 mm, 5 μm) and an UV detector set at 270 nm for phenol and catechol and 228 nm for benzoic acid. A RSLC C18 column (100 × 2 mm, 2.2 μm) was applied for evaluating the concentration of an antibiotic, sulfachloropyridazine (SCP). Methylene blue (MB) was determined on a JASCO UV–vis spectrophotometer at a wavelength of 664 nm. After each run, the passivated catalysts were recycled and washed with water and ethanol for 4 times each and dried in an oven at 60 °C overnight for reuse. Data in key figures were obtained from three parallel experiments to estimate the mean value and standard deviation. The initial rate constants were determined by a pseudo-first-order kinetic model in first 30 min before severe deactivation of the carbocatalysts.

2.3. Identification of reactive radicals

Electron paramagnetic resonance (EPR, Bruker) was utilized to probe the radical generation process during PS activation and the reactive radicals were trapped by 5, 5-dimethylpyrroline-oxide (DMPO, 0.08 M). The EPR instrument was operated at the centre field of 3514.8 G, sweep width of 100.0 G and power of 18.7 mW with sweeping time of 30 s.

2.4. Electrochemical measurement

The electrochemical study was performed in O_2-saturated KOH (0.1 M) solution. A standard three-electrode configuration was utilized with an Ag/AgCl (4 M KCl) as a reference electrode, a platinum wire as a counter electrode, and a catalyst-coated glassy carbon rotating disk electrode as a working electrode (GC-RDE, 0.196 cm^2, Pine Research Instrumentation, USA). The catalyst suspension was prepared by sonication of 5 mg of electrocatalyst, 2.5 mL of absolute ethanol and 0.25 mL of Nafion® solution (5.0 wt% in isopropanol and water solution) for 2 h. Then 40 μL of the as-prepared suspension was pipetted onto GC-RDE. At last, the catalyst layer on the GC electrode was dried in air overnight before use. Electrochemical data were obtained on a CHI instrument (CHI 760E series Bipotentiostat, USA). Cyclic voltammogram (CVs) measurements were conducted at a scan rate of 100 mV s^{-1} from 0.2 to −1.0 V *vs.* Ag/AgCl. Linear sweep voltammograms (LSVs) were acquired at a scan rate of 5 mV s^{-1} from 0.2 to −0.6 V *vs.* Ag/AgCl on the RDE (1600 rpm). Electrochemical impedance spectroscopy (EIS) was carried out utilizing a 5 mV amplitude AC voltage (frequency range from 10^5 to 10^{-1} Hz) and acquired at −0.3 V *vs*. Ag/AgCl.

3. Results and discussion

3.1. Characterization of NDs

TEM images in Fig. 1a and b demonstrate that after removal of amorphous carbon layers, smaller size particles with a characteristic core/shell structure were obtained for the annealed nanodiamond. The fingerprints in diamond crystals indicated a d-spacing of 2.06 Å, which was in a good agreement of the selected area electron diffraction (SAED) patterns (inset) and the sharp peak at the 2θ of 42.5° in XRD spectra (Fig. 1c) corresponding to the (111) diamond facet. Electron energy loss spectroscopy (EELS) was applied to further probe the carbon type of the annealed nanodiamond with the carbon K-edge spectra at the diamond core and graphitic shell (Fig. 1d). The σ* transition peak at 293.3 eV originated from C 1s electrons of the sp^3 hybridized diamond core structure, whereas the peak at 285.5 eV can be attributed to the π* transition of the sp^2 hybridized graphitic shell, confirming the hybrids of AND-1000 [36,37]. The SSAs (specific surface areas, Table S1) and adsorption volume (Fig. 2c, d) slightly increased for AND-1000, while the thermal stability of the nanodiamonds slightly increased after the pyrolysis in nitrogen (as shown in Fig. 2b), due to the transformation of the core structure to more stable graphitic outer shell. Thermal annealing of nanodiamonds consists of complicated processes including the decomposition of surface functional groups, collapse of diamond-edge plane (001) and reconstruction into graphitic plane (001), and formation of novel nanohybrid structure [35,38]. FTIR spectra in Fig. 2a suggests that most of functional groups on pristine NDs were removed after the pyrolysis. X-ray photoelectron spectroscopy (XPS) surveys (Fig. S1) indicate that the oxygen level decreased after the thermal treatment due to removal of excess functional groups. The minor nitrogen impurity was introduced during the denotation process of ND manufacture.

3.2. Catalytic evaluation of NDs and metal oxides

In oxidative reaction, persulfate without activation is ineffective for phenol degradation (Fig. S2). As illustrated in Fig. 3a, phenol oxidation was dramatically enhanced on modified NDs compared to that on pristine NDs. The initial rate constants of pristine ND and AND-1000 were estimated to be 0.004 and 0.084 min^{-1} (Fig. S3), and a 21-fold enhancement in the activity was achieved on the AND-1000. Fig. S4 also suggests that AND-1000 is more efficient in persulfate activation for SCP oxidation. The reaction pathways were revealed by identification of reaction intermediates (Figs. S5 and S6), *e.g.* 1,4-hydroquinone, benzoquinone, and mineral acids. Phenol was first partially oxidized to the phenolic derivatives, then transformed into smaller molecular acids *via* a series of ring-opening, H abstraction, and addition reactions. This is further confirmed by the decreased pH of the reaction solution from 5.9 (initial) to 3.3 when phenol was completely oxidized as shown in Fig. S7. It has been reported that metal oxides such as Fe_3O_4 and core–shell Fe–Fe_2O_3 could activate persulfate for catalytic degradation of dyes and pharmaceuticals [39,40]. In this study, catalytic oxidation of phenol on AND-1000 with PS activation was much more efficient than most popular metal oxides as indicated in Fig. 3b. Compared with the metal oxide particles, the diamond nanocrystals possess a higher surface to volume ratio and exhibit better access to the reactants, which would not only facilitate the adsorption process but also expose more active sites for catalytic reactions. Nevertheless, the reaction rate of zero valent iron (ZVI) is slightly faster than that of AND-1000 with 100% phenol oxidation in 20 min, the severe deactivation (seen in Fig. S8) due to surface coverage of ferric hydroxide and irreversible leaching of excessive iron ions from ZVI significantly impede the application for green remediation. Such metal-free catalytic oxidation can also be used for effective degradation of an antibiotic (sulfachloropyridazine, SCP), dye (methylene blue, MB), and catechol (Fig. S9).

The pristine nanodiamonds produced from the detonation method present a characteristic core/shell structure which is partially covered by soots and amorphous carbon and can be modified with versatile functional groups [41,42]. The thermal annealing processes are believed to be capable of removing the inert coatings, facilitating the formation of an onion-like graphitic shell due to the collapse and transformation of the diamond (001) surface [35]. The unique sp^3/sp^2 hybrids possess the chemical properties of graphene with various surface defects and can induce intricate interactions with the diamond core, thus having demonstrated excellent catalytic performances in various redox reactions such as oxygen reduction reaction (ORR), selective oxidation and oxidative dehydrogenation reactions [29,34,35,37]. In this study, pristine NDs present a poor activity for PS activation. The dramatic improvement was achieved after the thermal annealing, suggesting that the graphitic shell structure of AND-1000 functionalized with the surface defects can effectively interact with PS for activation of O—O bond and generation of reactive species. The removal of nonreactive amorphous carbon and functional groups significantly tuned the surface reducibility, which was beneficial to the electron-transfer process. Besides, the defective edges at the termination of sp^2 hybridized graphitic shell have been proposed to possess unique electronic states with delocalized π electrons due to the break of perfect hexagonal cell, herein presenting a superb capability for catalytic reactions especially for redox processes [29,43]. Moreover, the curvature of graphitic shell, similar to carbon nanotubes, was believed to be able to expose certain amounts of σ electrons. Distinct from other nanocarbons such as graphene or carbon nanotubes, the sp^3-hybridized diamond core may also deliver electrons to the shell structure *via* covalent bonding, then synergistically facilitating the water bonding and persulfate activation. It is well known that further increasing the annealing temperature (over 1700 °C) would completely transfer the diamond core into graphitic and onion-like shell construction, thus the annealing temperature would effectively tailor the ratio and thickness of core/shell hybrids [44]. The electrochemical activity of carbon nanotubes was reported to strongly depend on the wall/layer numbers and further increasing the thickness of the walls (>2 layers) is not favorable for charge transport due to the diminished distribution of DC bias, the inner driving force [45]. Therefore, the electron tunnelling effect between the multiple shells and core/shell interfaces

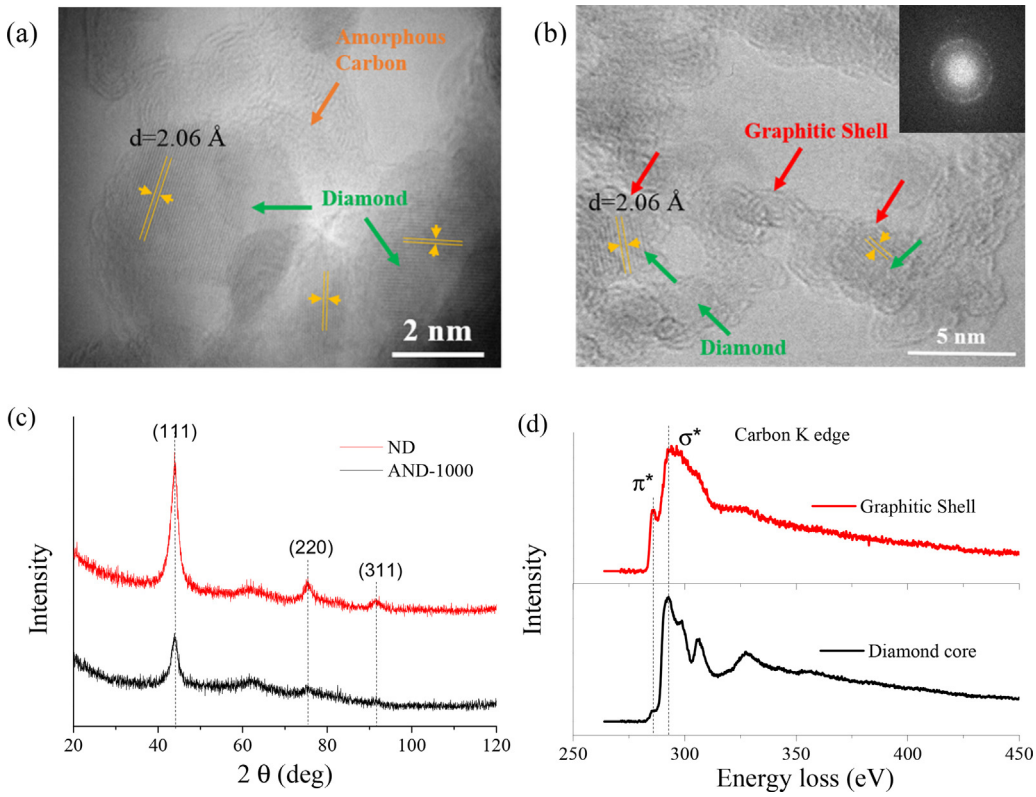

Fig. 1. HRTEM images of (a) ND and (b) AND-1000 (SAED pattern, inset), (c) XRD patterns of ND and AND-1000, (d) EELS carbon K-edge spectra of the core and shell structures of AND-1000.

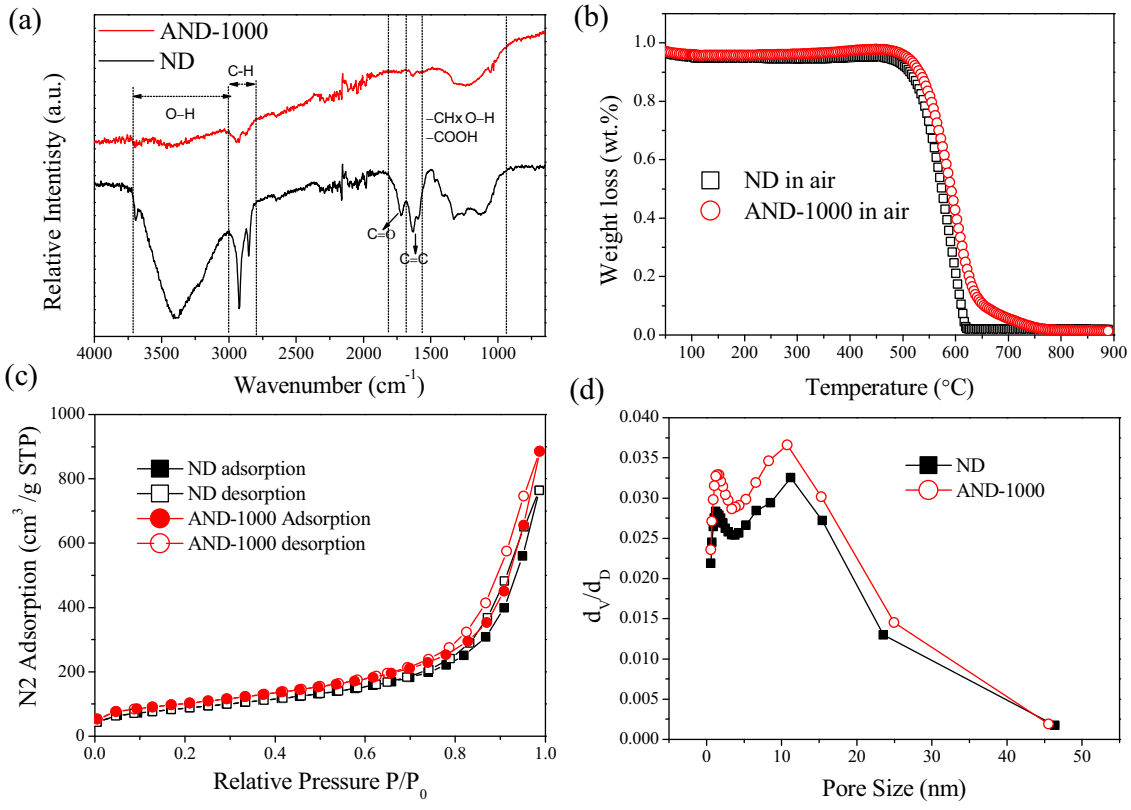

Fig. 2. (a) FTIR spectra, (b) TGA curves, (c) nitrogen sorption profiles, and (d) pore size distributions of pristine ND and AND-1000.

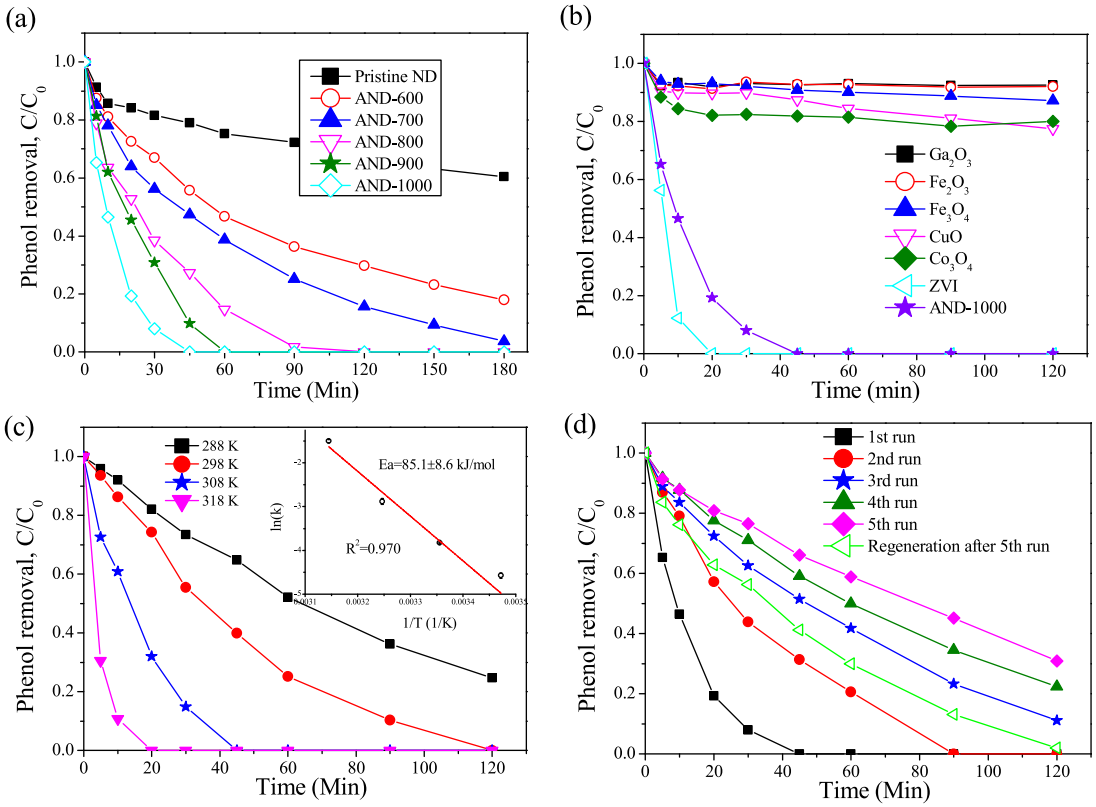

Fig. 3. (a) Phenol oxidation with carbocatalysts, (b) PS activation on AND-1000, ZVI, and various metal oxides, (c) Influence of temperature on phenol oxidation (catalyst = 0.1 g/L), and (d) Recyclability tests of AND-1000.

of nanodiamonds could be manipulated by adjusting the annealing temperature to achieve the optimized composite structure with the best catalytic activity toward metal-free catalysis.

Electrochemical measurement was performed to probe the charge transfer process at the interface of water/PS/nanodiamond and compare the redox potential on different carbocatalysts. Electrochemical impedance spectroscopy (EIS) analysis in Fig. 4a indicates that AND-1000 presented a smaller semicircle diameter, suggesting the thermal annealing process considerably improved the charge transfer capability of the nanodiamond due to the formation of the sp^2-hybridized graphitic shell. The cyclic voltammetry (CV) performance of nanodiamonds in Fig.4b further demonstrates that AND-1000 presented a greater reduction capacity for chemical reactions and redox processes in PS (6.5 mM) and Na_2SO_4 (0.1 M) solutions [46]. Moreover, it is supposed that the PS activation process by NDs is similar to ORR on carbocatalysts, in which the O—O bonds in oxygen molecules are first activated by the carbon surface and then broken up by obtaining electrons from the electrode to form H_2O_2 (two-electron pathway) or OH^- (four-electron pathway) [47,48]. The promoted ORR performance on the AND-1000 (Fig. S10) also confirmed the enhanced catalysis in charge transfer and O—O bond activation.

The effects of initial phenol concentration, catalyst loading, and dosage of PS on phenol degradation in corresponding kinetic behaviors are shown in Figs. S11 and S12 . Different from initial phenol concentration and catalyst loading, the increase of PS loading shows a negligible influence on the degradation efficiency. This might be ascribed to the limited active sites (defects) on nanodiamonds during PS activation and self-quenching effect among the excessive radicals. Fig. 3c indicates that 75.4% phenol removal was attained at 15 °C in 120 min, while complete phenol oxidation was attained on AND-1000 at 25 °C, and the time for complete phenol decomposition reduced to 45 and 20 min at 35 and 45 °C, respectively. The influence of reaction temperature on PS activation by annealed nanodiamonds is more significant than that by graphene-based materials and carbon nanotubes reported before [13,15]. The activation energy of phenol degradation on AND-1000 was evaluated to be 85.1 ± 8.1 kJ/mol, which is higher than that on the multi-walled carbon nanotubes (44.6 kJ/mol) [15]. As physical approaches such as heat or UV are reported to be capable of activating PS to generate sulfate radicals for oxidation, the effect of reaction temperature without carbocatalysts is also provided in Fig. S13. It can be seen that the influence of temperature is insignificant giving 1.9 and 4.4% phenol oxidation in 120 min at 25 and 35 °C, respectively, while 19.6 and 81.7% phenol removals were yielded at 45 and 100 °C, respectively. Therein, the improved oxidative effectiveness at low temperature was mostly attributed to the enhanced catalytic effect of AND-1000/PS system. The sp^3-hybridized core demonstrated a superior thermal conductance from the diamond core to the shell and was beneficial for endothermic processes for phenol adsorption and oxidation, meanwhile facilitating the electron conduction from the core to shell and charge transfer on the nanodiamond surface [29].

In the previous studies, the reusability of metal catalysts for PS activation was rarely discussed, due to the irreversibility of homogeneous metal ions, severe metal-leaching and surface coverage of ferrous sulfate or ferric hydroxide on ZVI-based heterogeneous catalysts [11,49]. The deactivation of the carbocatalysts is mainly due to the coverage of adsorbed intermediates, altered surface chemistry, minor change of pore structure, and oxidation or destruction of carbocatalysts in the highly oxidative environment with hydroxyl radicals [50–52]. Both XPS and FTIR spectra confirmed the increased oxygen level of the carbocatalyst (Fig. S1 and Fig. S14) after the first run due to the surface oxidation and intermediates adsorption, meanwhile the SSA and pore volume slightly decreased owing to the change of pore structure

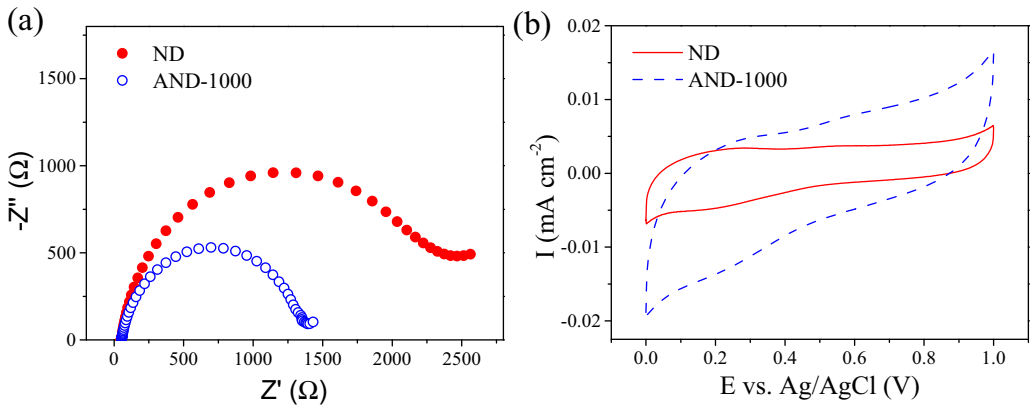

Fig. 4. (a) EIS plots of ND and AND-1000 electrodes recorded at −0.3 V *vs.* Ag/AgCl under the influence of an AC voltage of 5 mV amplitude in 0.1 M KOH solution; (b) CVs of ND and AND-1000 catalysts in PS and Na_2SO_4 solution after 10 cycles. (Scan rate: 50 mV s^{-1}, [Na_2SO_4] = 0.1 M, [PS] = 6.5 mM, RDE rotating rate: 0 rpm, N_2 saturated).

and coverage of active sites (Fig. S15). We recently observed that carbon nanotubes demonstrated excellent activity and reusability in PMS activation owing to the highly graphitic and curved graphene shell structure [53]. In this study, the AND-1000 demonstrated an excellent reusability providing 100% phenol oxidation in the 2nd run. Moreover, 89.0, 77.6, and 69.1% phenol removal efficiencies were attained in 120 min in the 3rd, 4th, and 5th runs, respectively (Fig. 3d). The stability of the surface-tuned nanodiamond is much better than chemically modified graphene, carbon nanotubes, cubic ordered mesoporous carbon (CMK-8) and activated carbon [17]. The better stability of the annealed nanodiamonds might be ascribed to the robust core-shell (sp^3/sp^2) hybrid structure, which exhibits a greater resistance to oxidation than graphene- or CNT- based systems. The deactivated AND-1000 after the 5th run was regenerated with a thermal treatment (annealing at 300 °C under nitrogen atmosphere for 1 h). The activity of passivated carbocatalyst was recovered with 98.1% phenol removal in 120 min due to the removal of adsorbed intermediates and tuning of oxidized diamond surface. It should be noted that the stability of the current carbocatalysis-based AOPs system is still not comparable to many commercial metal-based systems such as electrochemical catalysis and dehydrogenation reactions. Therefore, intensive efforts are needed to provide efficient and robust materials for metal-free catalysis for future applications.

3.3. Mechanism of radical evolution on nanodiamond

EPR was employed to *in situ* detect the active species produced from PS activation on nanodiamonds. Fig. 5a indicates that the radical intensity of AND-1000 is higher than that of pristine nanodiamond, suggesting a better capability of the AND-1000 to activate PS to generate free radicals. It was already known that homogeneous Fe^{2+}/PS reaction would primarily produce sulfate radicals ($SO_4^{\bullet-}$) (Fig. 5b). The persulfate radicals may also contribute to organic oxidation especially in the presence of O_2 which cannot be ruled out in this study [54]. Huang et al. also reported that EPR spectra in persulfate activated system changed significantly due to the variation of PS/catalyst concentration and transition of major radical species (•OH and $SO_4^{\bullet-}$) along with the reaction time [55]. However, the nanodiamonds in this study were able to activate PS to mainly produce hydroxyl radicals (•OH) and minor amount of sulfate radicals were detected throughout the reaction (Fig. 5c and d), which was similar to the systems with PS activation on other nanocarbons such as graphene and carbon nanotubes in our previous studies [17]. Since persulfate (SO_3-O-O-SO_3) can be only decomposed to produce $SO_4^{\bullet-}$ and the transition from $SO_4^{\bullet-}$ to •OH should only contribute to a small portion of the produced

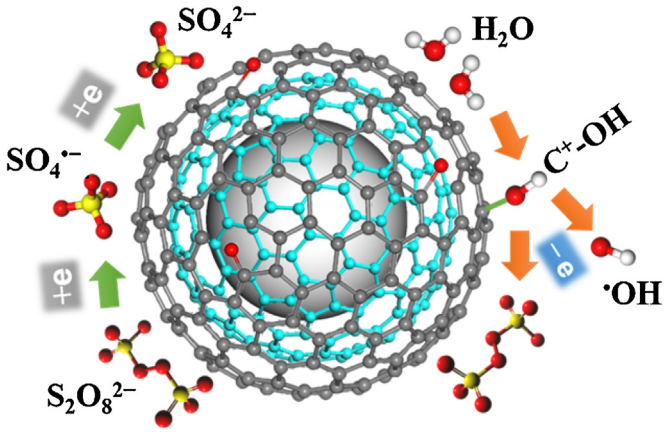

Scheme 1. Proposed mechanism of persulfate activation on annealed nanodiamonds.

•OH, the generation of hydroxyl radicals should be induced from water oxidation. As the persulfate alone with an oxidation potential of 1.96 V (NHE) cannot directly oxidize water molecules (OH/H_2O −2.8 V, NHE) in thermodynamics [56], PS may be first activated by the graphitic shell of the carbocatalyst and then oxidize the adsorbed water *via* one-electron transfer process. The phenomenon is intrinsically distinct from ferrous ions and ZVI systems [17]. In a recent study, we first carried out density functional theory (DFT) calculations to reveal the PS activation process on carbocatalysts [57]. We found that when water was presented adjacent to a persulfate molecule on the surface of a carbocatalyst, the H—O bond in H_2O was significantly lengthened with greater tendance to donate electrons to the carbon matrix, meanwhile the persulfate molecule demonstrated enhanced adsorption energy, prolonged the O—O bond, more charge transfer from the catalyst, suggesting the oxidation of water by PS and generation of hydroxyl radicals. Interestingly, we further discovered that the oxidation efficiencies of both benzoic acid (BA) and nitrobenzene (NB), which are more readily to react with hydroxyl radicals than sulfate radicals, are quite low as demonstrated in Fig. S16. The results suggest that sulfate radicals could still be the dominant reactive species in this oxidative system. The oxidized water molecules on the surface of carbocatalyst may be able to not only generate hydroxyl radicals, but also act as a significant intermediate for persulfate activation to generate sulfate radicals as elucidated in Scheme 1. The similar catalytic phenomenon was also reported in the base and cobalt-based oxidative processes [4,6,58]. The surface-bonded sulfate radical would quickly react with the target organics and then present rel-

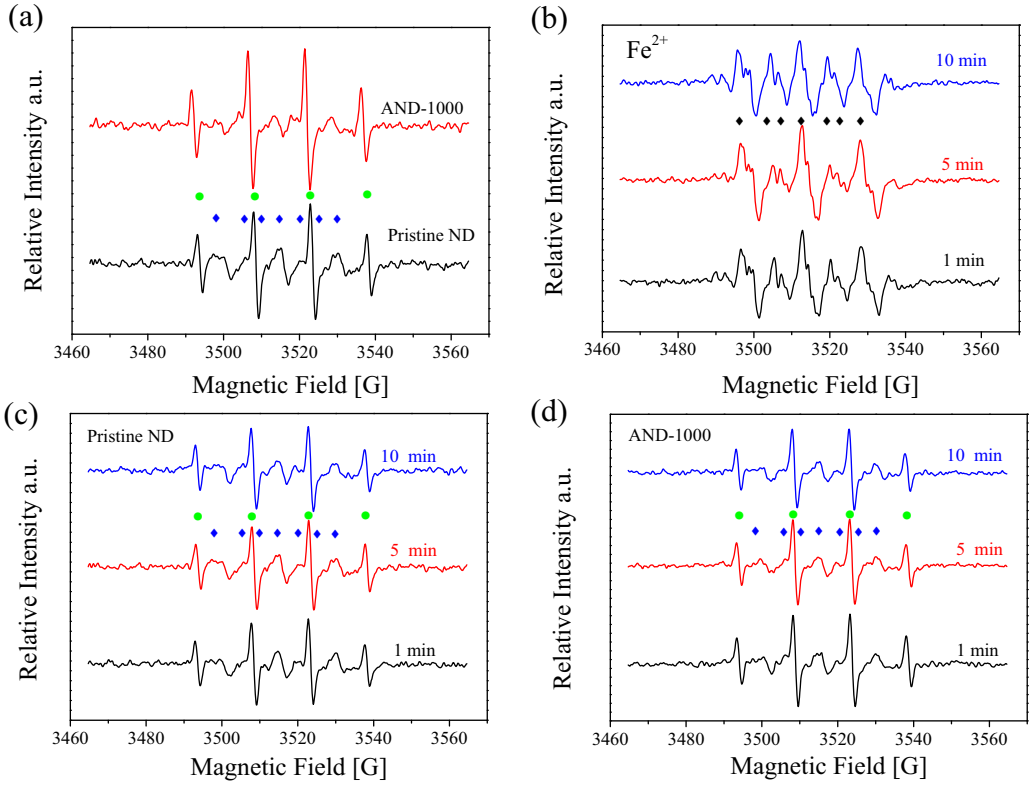

Fig. 5. (a) Comparison of EPR spectra of PS activation on pristine nanodiamond and AND-1000. EPR spectra of active radicals induced by (b) homogeneous PS activation with Fe^{2+} and heterogeneous activation on (c) pristine NDs and (d) AND-1000. (●: DMPO-OH, ♦: DMPO-SO_4).

ative low response in the EPR spectra. As the transient state of the catalytic process is complicated and difficult to be revealed by experiment here, a combination of advanced *in situ* characterization techniques and theoretical calculations are still required to explore the reaction pathways in future studies.

To further verify the proposed process, the effect of solution pH on PS activation was investigated. Fig. 6a shows that phenol degradation on AND-1000/PS system is favored at the basic condition and phenol oxidation efficiency enhances with the elevated pH values. As the decomposed persulfate and phenol may rapidly acidify the solution due to formation of H_2SO_4 and mineralized acids, buffered solutions were also applied to verify the effect of basic conditions as indicated in Fig. S18. It was found that phenol can be quickly removed in less than 10 min under buffered conditions (pH = 10.0–11.5) without a significant pH change, whereas the basic conditions without a carbocatalyst can only provide 18.9% phenol removal in 60 min. Since a hydroxide ion with bare extra electrons is more easily to donate an electron to PS without activation of H—O bond compared with water molecules to form hydroxyl radicals, the higher pH is favorable for PS activation on a carbocatalyst. Moreover, AND-1000 remained high catalytic activity for PS activation in a much wider pH range (pH 2–11), compared with the conventional Fenton reactions (H_2O_2, pH < 3), ozone- (O_3), and peroxymonosulfate- (neutral and basic conditions) based oxidative reactions [19,59,60]. It should be pointed out that the basic condition was also reported to be able to induce PS decomposition, yet not significant for phenol oxidation in this study with only 6.3 and 18.9% phenol removal in an unbuffered and buffered basic conditions, respectively [6]. The heterogeneous carbocatalysis may be more effective than base activation for stimulating persulfate to generate reactive species. Besides, the formation of phenoate species in the basic condition may impact the reactivity of phenol and intermediates in the oxidative processes.

Recent studies indicated that nonradical oxidation might occur in PMS and PS activation and the existence of radical quenching agents did not remarkably affect the performances of organic decomposition in the oxidative systems [53,61]. Fig. 6b shows that phenol removal efficiency and reaction rate constants decreased dramatically at high ratios of ethanol (a scavenger of hydroxyl and sulfate radicals), suggesting the critical roles of radicals in the oxidation. Moreover, when the aqueous solution was completely replaced with ethanol (only 1% water remaining introduced in phenol stock solution), the oxidation was almost completely terminated which is intrinsically distinctive from the nonradical dominated processes (Fig. S19). It should be noteworthy that ethanol might also function as an electron donor (competing with water) to prevent the radical formation rather than a radical scavenger to donate one electron transfer to persulfate *via* AND surface, hereby slowing down the oxidation rate.

3.4. Influence of natural organic matter and halogen ions

In a real wastewater matrix, the background organic matters and various radical scavengers would severely affect the organic degradation effectiveness [21]. Natural organic matters (NOMs), such as humic acid (HA), are rich in electrons and can serve as an oxidant scavenger to react with the reactive radicals, thus significantly decreasing the oxidation efficiency toward target contaminants. On the other hand, the NOMs with semiquinone radicals (phenols, quinones, and hydroquinones) were also reported to be able to mediate PMS and PS to generate $^{\bullet}OH$ and $SO_4^{\bullet-}$ [8,9,12,60]. Fig. 6c indicates that the presence of HA at low concentrations presented a marginal impact on PS activation and phenol oxidation on AND-1000. The PS/AND-1000 system showed high-efficiency in phenol removal from wastewater in the presence of natural organic matters though the hydroxyl radicals were reported to be non-selective

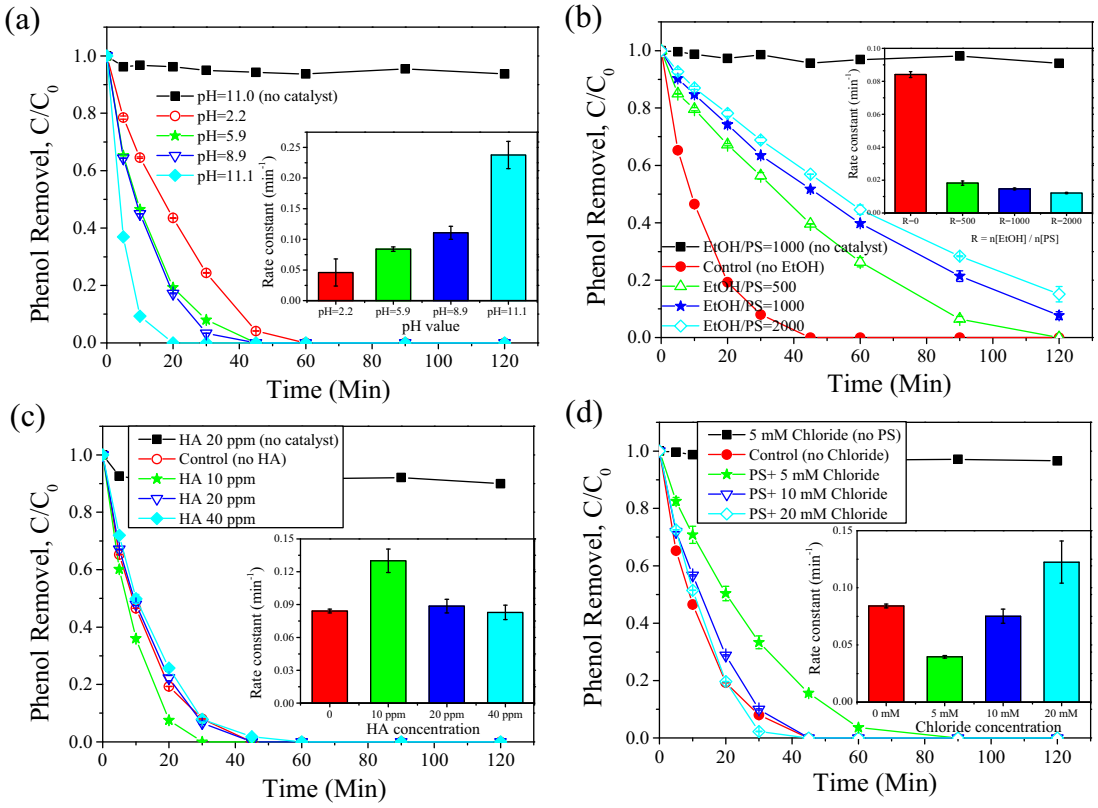

Fig. 6. Influences of (a) pH, (b) ethanol, (c) humic acid, and (d) chloride on phenol oxidation with PS/AND-1000.

[21,62]. The PS/AND-1000 can generate a myriad of free radicals that are capable of attacking phenol and HA simultaneously. Moreover, the phenol removal efficiency degreased gradually with increasing addition of HA (Fig. S19) due to the competing reaction of HA with hydroxyl radicals (Fig. S20) and insufficiency of the oxidants.

The influence of chloride ions in solution on catalytic phenol degradation is shown in Fig. 6d. The presence of a minor amount of chloride ions results in a declined efficiency of phenol degradation because the chloride ions scavenge most of the sulfate radicals and a small part of hydroxyl radicals to form Cl• and $Cl_2^{\bullet-}$, which are less reactive than $SO_4^{\bullet-}$ and •OH. However, superabundant chloride ions (Cl^-) in the solution will not only shield $SO_4^{\bullet-}$ and •OH, but compete with the adsorbed water molecules to donate electrons on the carbon surface to PS to form Cl• that subsequently combines another Cl^- to produce $Cl_2^{\bullet-}$. This procedure is similar to the hydroxyl radical generation *via* oxidizing water with PS on the carbocatalysts. Besides, the generated myriad amounts of •OH can also react with Cl^- to produce Cl• and $Cl_2^{\bullet-}$ (Eqs. (3)–(5)) in an acid condition. It was interesting to notice that introducing minor amount of chloride ions would slow down the reaction rate from 0.084 (0 mM Cl^-) to 0.040 min^{-1} (5 mM Cl^-), whereas the rate constants gradually increased to 0.075 and 1.122 min^{-1} when 10 mM and 20 mM Cl^- were added into the oxidative system, respectively. The excess $Cl_2^{\bullet-}$ can mineralize the electron-rich phenol and intermediates such as diphenols and benzoquinone, giving rise to an enhanced efficiency of phenol removal *via* H-abstraction and one-electron oxidation [20–22]. It should be noted that the halogenated compounds such as dichlorophenols and trichlorophenols, which are produced from phenol mineralization and similar to disinfection by-products, are highly toxic and more resistant to be degraded in the advanced oxidation. The process should be controlled and optimized in future applications.

4. Conclusions

In summary, annealed nanodiamonds were discovered to be able to activate persulfate to produce both hydroxyl and sulfate radicals. The water oxidation process and formation of transient intermediates on the surface of the carbocatalyst may act significant roles in persulfate activation. Such emerging catalysis demonstrated potentials for overcoming the demerits of both sulfate and hydroxyl radical-based reactions. The annealed graphitic core-shell structure with versatile defects of ANDs provides a fantastic environment for oxygen and PS activation by serving as a superb bridge for charge transfer. Besides, the intricate interactions of sp^2 and sp^3 interfaces *via* conjugation effects are able to induce electron transport from the nanodiamond core to shell surface, further enhancing the O-O breakup efficiency. Thus, AND/PS provides an excellent route for organic oxidation, which can be applied for contaminant decomposition and selective oxidation reactions by carbocatalysis. As ANDs are mainly synthesized *via* a detonation method and modified with thermal treatments, the high-cost of the carbocatalysts compared with conventional transition metals or metal oxides severely limits their wide application to environmental engineering. Thus, state-of-the-art strategies are still needed to be developed for preparation of efficient and cheap diamond-based carbocatalysts. In regard to future environmental implications, the novel oxidative system (PS/AND) should be evaluated for degradation of versatile persistent contaminants such as antibiotics (*e.g.* SCP in this study), pharmaceuticals, personal-care products, and endocrine disruption compounds. Moreover, the interference and impact of various natural organic matters (*e.g.* HA), radical scavengers (halogen ions) and potential byproducts should also be evaluated in the future studies.

Acknowledgement

The authors acknowledge the financial support from Australian Research Council (ARC-DP130101319) and H. S. appreciates the support from Curtin Research Fellowship.

Appendix A. Supplementary data

Supplementary data associated with this article can be found, in the online version, at http://dx.doi.org/10.1016/j.apcatb.2016.04.043.

References

[1] S. Navalon, R. Martin, M. Alvaro, H. Garcia, Angew. Chem. Int. Ed. 49 (2010) 8403–8407.
[2] B. Ensing, F. Buda, P. Blochl, E.J. Baerends, Angew. Chem. Int. Ed. 40 (2001) 2893–2895.
[3] X.W. Liu, X.F. Sun, D.B. Li, W.W. Li, Y.X. Huang, G.P. Sheng, H.Q. Yu, Water Res. 46 (2012) 4371–4378.
[4] G.P. Anipsitakis, D.D. Dionysiou, Environ. Sci. Technol. 37 (2003) 4790–4797.
[5] T. Zhang, Y. Chen, Y.R. Wang, J. Le Roux, Y. Yang, J.P. Croue, Environ. Sci. Technol. 48 (2014) 5868–5875.
[6] O.S. Furman, A.L. Teel, R.J. Watts, Environ. Sci. Technol. 44 (2010) 6423–6428.
[7] J. Kronholm, M.L. Riekkola, Environ. Sci. Technol. 33 (1999) 2095–2099.
[8] G.D. Fang, J. Gao, D.D. Dionysiou, C. Liu, D.M. Zhou, Environ. Sci. Technol. 47 (2013) 4605–4611.
[9] M. Ahmad, A.L. Teel, R.J. Watts, Environ. Sci. Technol. 47 (2013) 5864–5871.
[10] S. Ahn, T.D. Peterson, J. Righter, D.M. Miles, P.G. Tratnyek, Environ. Sci. Technol. 47 (2013) 11717–11725.
[11] P. Drzewicz, L. Perez-Estrada, A. Alpatova, J.W. Martin, M.G. El-Din, Environ. Sci. Technol. 46 (2012) 8984–8991.
[12] G.D. Fang, C. Liu, J. Gao, D.D. Dionysiou, D.M. Zhou, Environ. Sci. Technol. 49 (2015) 5645–5653.
[13] X.G. Duan, Z.M. Ao, H.Q. Sun, S. Indrawirawan, Y.X. Wang, J. Kang, F.L. Liang, Z.H. Zhu, S.B. Wang, ACS Appl. Mater. Interfaces 7 (2015) 4169–4178.
[14] H.Q. Sun, S.Z. Liu, G.L. Zhou, H.M. Ang, M.O. Tade, S.B. Wang, ACS Appl. Mater. Interfaces 4 (2012) 5466–5471.
[15] H.Q. Sun, C. Kwan, A. Suvorova, H.M. Ang, M.O. Tade, S.B. Wang, Appl. Catal. B 154 (2014) 134–141.
[16] X. Wang, Y. Qin, L. Zhu, H. Tang, Environ. Sci. Technol. 49 (2015) 6855–6864.
[17] X.G. Duan, H.Q. Sun, J. Kang, Y.X. Wang, S. Indrawirawan, S.B. Wang, ACS Catal. 5 (2015) 4629–4636.
[18] H.Q. Sun, Y.X. Wang, S.Z. Liu, L. Ge, L. Wang, Z.H. Zhu, S.B. Wang, Chem. Commun. 49 (2013) 9914–9916.
[19] Y. Yang, J. Jiang, X. Lu, J. Ma, Y. Liu, Environ. Sci. Technol. 49 (2015) 7330–7339.
[20] G.P. Anipsitakis, D.D. Dionysiou, M.A. Gonzalez, Environ. Sci. Technol. 40 (2006) 1000–1007.
[21] J.E. Grebel, J.J. Pignatello, W.A. Mitch, Environ. Sci. Technol. 44 (2010) 6822–6828.
[22] Y. Yang, J.J. Pignatello, J. Ma, W.A. Mitch, Environ. Sci. Technol. 48 (2014) 2344–2351.
[23] X. Sun, Y. Ding, B. Zhang, R. Huang, D. Chen, D.S. Su, ACS Catal. 5 (2015) 2436–2444.
[24] S. Osswald, G. Yushin, V. Mochalin, S.O. Kucheyev, Y. Gogotsi, J. Am. Chem. Soc. 128 (2006) 11635–11642.
[25] O. El Tall, Y.F. Hou, E. Abou-Hamad, I.U. Raja, M.N. Hedhili, W. Peng, R. Mahfouz, O.M. Bakr, P.M. Beaujuge, Chem. Mater. 26 (2014) 2766–2769.
[26] D. Zhu, L.H. Zhang, R.E. Ruther, R.J. Hamers, Nat. Mater. 12 (2013) 836–841.
[27] D.M. Jang, Y. Myung, H.S. Im, Y.S. Seo, Y.J. Cho, C.W. Lee, J. Park, A.Y. Jee, M. Lee, Chem. Commun. 48 (2012) 696–698.
[28] G.D. Wen, S.C. Wu, B. Li, C.L. Dai, D.S. Su, Angew. Chem. Int. Ed. 54 (2015) 4105–4109.
[29] J. Zhang, D.S. Su, R. Blume, R. Schlogl, R. Wang, X.G. Yang, A. Gajovic, Angew. Chem. Int. Ed. 49 (2010) 8640–8644.
[30] J. Diao, Z. Feng, R. Huang, H. Liu, S.B.A. Hamid, D.S. Su, ChemSusChem (2016), http://dx.doi.org/10.1002/cssc.201501516.
[31] H. Ba, S. Podila, Y.F. Liu, X.K. Mu, J.M. Nhut, V. Papaefthimiou, S. Zafeiratos, P. Granger, C. Pham-Huu, Catal. Today 249 (2015) 167–175.
[32] H. Ba, L. Truong-Phuoc, Y.F. Liu, C. Duong-Viet, J.M. Nhut, L. Nguyen-Dinh, P. Granger, C. Pham-Huu, Carbon 96 (2016) 1060–1069.
[33] J. Zhang, D.S. Su, A.H. Zhang, D. Wang, R. Schlogl, C. Hebert, Angew. Chem. Int. Ed. 46 (2007) 7319–7323.
[34] X. Liu, B. Frank, W. Zhang, T.P. Cotter, R. Schlogl, D.S. Su, Angew. Chem. Int. Ed. 50 (2011) 3318–3322.
[35] Y.M. Lin, D.S. Su, ACS Nano 8 (2014) 7823–7833.
[36] S. Turner, O.I. Lebedev, O. Shenderova, I.I. Vlasov, J. Verbeeck, G. Van Tendeloo, Adv. Funct. Mater. 19 (2009) 2116–2124.
[37] Y.M. Lin, X.L. Pan, W. Qi, B.S. Zhang, D.S. Su, J. Mater. Chem. A 2 (2014) 12475–12483.
[38] V.L. Kuznetsov, A.L. Chuvilin, Y.V. Butenko, S.V. Stankus, R.A. Khairulin, A.K. Gutakovskii, Chem. Phys. Lett. 289 (1998) 353–360.
[39] L.L. Zhu, Z.H. Ai, W.K. Ho, L.Z. Zhang, Sep. Purif. Technol. 108 (2013) 159–165.
[40] J.C. Yan, M. Lei, L.H. Zhu, M.N. Anjum, J. Zou, H.Q. Tang, J. Hazard. Mater. 186 (2011) 1398–1404.
[41] V.N. Mochalin, O. Shenderova, D. Ho, Y. Gogotsi, Nat. Nanotechnol. 7 (2012) 11–23.
[42] A. Krueger, J. Mater. Chem. 18 (2008) 1485–1492.
[43] D.E. Jiang, B.G. Sumpter, S. Dai, J. Chem. Phys. 126 (2007) 134701.
[44] M. Zeiger, N. Jackel, V.N. Mochalin, V. Presser, J. Mater. Chem. A 4 (2016) 3172–3196.
[45] Y. Cheng, C.W. Xu, L.C. Jia, J.D. Gale, L.L. Zhang, C. Liu, P.K. Shen, S.P. Jiang, Appl. Catal. B 163 (2015) 96–104.
[46] Y.M. Ren, L.Q. Lin, J. Ma, J. Yang, J. Feng, Z.J. Fan, Appl. Catal. B 165 (2015) 572–578.
[47] Y. Zheng, Y. Jiao, J. Chen, J. Liu, J. Liang, A. Du, W.M. Zhang, Z.H. Zhu, S.C. Smith, M. Jaroniec, G.Q. Lu, S.Z. Qiao, J. Am. Chem. Soc. 133 (2011) 20116–20119.
[48] Y. Zhao, L.J. Yang, S. Chen, X.Z. Wang, Y.W. Ma, Q. Wu, Y.F. Jiang, W.J. Qian, Z. Hu, J. Am. Chem. Soc. 135 (2013) 1201–1204.
[49] M.A. Al-Shamsi, N.R. Thomson, Ind. Eng. Chem. Res. 52 (2013) 13564–13571.
[50] X. Duan, K. O'Donnell, H. Sun, Y. Wang, S. Wang, Small 11 (2015) 3036–3044.
[51] W.C. Hou, S. BeigzadehMilani, C.T. Jafvert, R.G. Zepp, Environ. Sci. Technol. 48 (2014) 3875–3882.
[52] J.G. Radich, A.L. Krenselewski, J.D. Zhu, P.V. Kamat, Chem. Mater. 26 (2014) 4662–4668.
[53] X. Duan, H. Sun, Y. Wang, J. Kang, S. Wang, ACS Catal. 5 (2015) 553–559.
[54] K. Clarke, R. Edge, E.J. Land, S. Navaratnam, T.G. Truscott, Radiat. Phys. Chem. 77 (2008) 49–52.
[55] Z.F. Huang, H.W. Bao, Y.Y. Yao, W.Y. Lu, W.X. Chen, Appl. Catal. B 154 (2014) 36–43.
[56] A.J. Bard, R. Parsons, Standard potentials in aqueous solution, CRC Press, New York, 1985.
[57] X. Duan, Z. Ao, H. Sun, L. Zhou, G. Wang, S. Wang, Chem. Commun. 51 (2015) 15249–15252.
[58] X. Chen, X. Qiao, D. Wang, J. Lin, J. Chen, Chemosphere 67 (2007) 802–808.
[59] T. Zhang, H.B. Zhu, J.P. Croue, Environ. Sci. Technol. 47 (2013) 2784–2791.
[60] Y.H. Guan, J. Ma, Y.M. Ren, Y.L. Liu, J.Y. Xiao, L.Q. Lin, C. Zhang, Water Res. 47 (2013) 5431–5438.
[61] H. Lee, H.J. Lee, J. Jeong, J. Lee, N.B. Park, C. Lee, Chem. Eng. J. 266 (2015) 28–33.
[62] H. Lee, H.Y. Yoo, J. Choi, I.H. Nam, S. Lee, S. Lee, J.H. Kim, C. Lee, J. Lee, Environ. Sci. Technol. 48 (2014) 8086–8093.